

Single Carbon Nanotube Schottky Diode Microwave Rectifiers

Enrique D. Cobas, Steven M. Anlage, *Member, IEEE*, and Michael S. Fuhrer

Abstract—We report the fabrication of single and few-channel carbon nanotube (CNT) Schottky diodes on high-frequency compatible substrates using horizontally aligned CNT arrays and dissimilar metal contacts in a coplanar-waveguide geometry. Rectification of ac signals in the range of 100 MHz–40 GHz is examined and the observed cutoff frequencies are used to compute the Schottky junction capacitance of the devices, which is strongly CNT-length-dependent and appears dominated by stray capacitance between the CNT channel and metal electrode, in agreement with electrostatic simulations.

Index Terms—Carbon nanotubes (CNTs), impedance mismatch, microwave rectification, Schottky diodes.

I. INTRODUCTION

THE high-frequency properties of carbon nanotubes (CNTs) have been of interest to the academic community for some time due to their useful bandgap [1], [2], high sustainable transport current density [3], high carrier mobility [4], long mean-free path [5], [6], and small capacitances, all properties they exhibit at room temperature. In addition, these 1-D systems challenge some assumptions about device electrostatics and charge transport. Significant quantum capacitance and kinetic inductance [7] introduce novel device physics. Further, electron–electron interactions are inevitable in one dimension, the charge carriers cannot be described as electron-like (Fermi liquid), but instead are plasmon-like (Luttinger liquid [8]–[12]) and transport charge at a velocity that is significantly different than the Fermi velocity. These properties and novel phenomena point to the possibility of terahertz CNT devices, including transistors, amplifiers [13], and oscillators [14], [15].

Reviews of the theoretical expectations for the high-frequency properties of these nanostructures have been performed by Burke [16] and others [17]. One of the principal obstacles to the use of CNTs in high-frequency electronics is their high

individual impedance. The quantum of conductance for a single quantum channel can be calculated by integrating the density of states between source and drain potentials

$$I = \frac{e}{h} \int_{k_d}^{k_s} \frac{d\varepsilon(k)}{dk} dk = \frac{e}{h} \int_{\mu_d}^{\mu_s} d\varepsilon = \frac{e}{h} \varepsilon(\mu_s - \mu_d) = \frac{e^2 V_{SD}}{h} \quad (1)$$

where μ_s and μ_d are the source and drain potentials, k_s and k_d are the momenta of the states at energies of μ_s and μ_d , and V_{SD} is the source–drain voltage. Thus, the conductance of a quantum channel is limited to e^2/h independent of any materials parameters, even without scattering. Spin and band degeneracy in CNTs produce a total of four parallel quantum channels, yielding a minimum impedance of $h/4e^2 \sim 6.45 \text{ k}\Omega$ for a single CNT. The impedance mismatch with traditional 50- Ω equipment produces signal transmission factors below 10^{-4} . To avoid this problem, devices can be based on a large number of parallel CNT channels that provide a better match to the 50- Ω standard. Although obstacles remain in the control or sorting of nanotube types, this approach has produced promising results, including device cutoff frequencies up to 23 GHz [18] and intrinsic cutoff frequencies up to 80 GHz [19] in field-effect transistor (FET) geometries. However, using many parallel CNTs, especially of different types, may blur and obscure phenomena unique to these 1-D systems.

To characterize few-CNT systems at microwave frequencies, we must deal with the high-impedance mismatch between them and the macroscopic world. One approach proposed by Manohara *et al.* [20] is the creation of Schottky diodes using semiconducting CNTs (CNT-SDs). Manohara *et al.* fabricated diodes on SiO₂/Si, which was unsuitable for high-frequency characterization. In a previous study, we improved upon this approach by fabricating CNT Schottky diodes on quartz substrates using a patterned catalyst approach, and demonstrated rectification of microwave signals up to 18 GHz introduced in the far field and coupled somewhat uncontrollably to the device [21].

In this study, we improve upon our previous work by creating CNT-SDs from arrays of aligned CNTs prepared on quartz substrates with coplanar-waveguide (CPW) contacts. This arrangement enables us to probe electrical transport in CNTs as a function of frequency (up to our equipment limit of 40 GHz) with a good signal-to-noise ratio (SNR). The maximum operating frequency of these rectifiers, $(2\pi RC)^{-1}$, is determined by the channel resistance and junction capacitance. The latter is expected to be in the 10^{-18} F range [10], [22]–[25] and in parallel with a larger parasitic capacitance, making it difficult to measure experimentally. Here we use the high-frequency cutoff values

Manuscript received March 03, 2011; revised June 29, 2011; accepted July 08, 2011. Date of publication September 15, 2011; date of current version October 12, 2011. This work was supported in part by the U.S. Office of Naval Research through the Center for Applied Electromagnetics, University of Maryland at College Park.

E. D. Cobas was with the Department of Physics and the Center for Nanophysics and Advanced Materials, University of Maryland at College Park, College Park, MD 20742 USA. He is now with the U.S. Naval Research Laboratory (NRL), Washington, DC 20375 USA (e-mail: enrique.cobas@nrl.navy.mil).

S. M. Anlage and M. S. Fuhrer are with the Department of Physics and the Center for Nanophysics and Advanced Materials, University of Maryland at College Park, College Park, MD 20742 USA (e-mail: anlage@umd.edu; mfuhrer@umd.edu).

Color versions of one or more of the figures in this paper are available online at <http://ieeexplore.ieee.org>.

Digital Object Identifier 10.1109/TMTT.2011.2164548

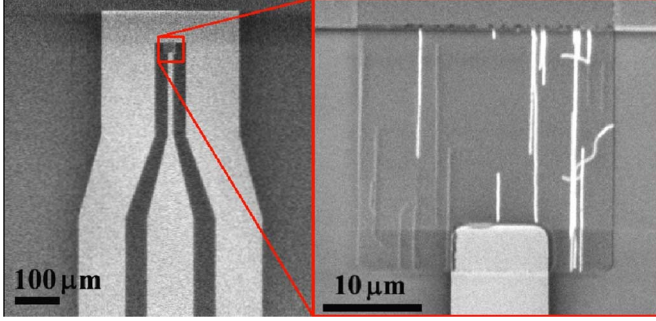


Fig. 1. (left) SEM image of the CPW electrode geometry and (right) close-up of the active device area. The center electrode (bottom feature on the close-up) is the Schottky contact, while the outer electrode (top in the close-up) is ohmic.

observed to extract the junction capacitance C_J , as a function of bias, channel length, and ambient doping.

II. DEVICE FABRICATION

Horizontally aligned arrays of CNTs were synthesized via chemical vapor deposition (CVD) using ferritin catalyst on st-cut quartz substrates following the approach of Kocabas *et al.* [26]. A further detailed review of synthesis parameters was performed by Routstka *et al.* [27]. Conventional photolithography was used to pattern an array of 50- Ω CPW electrodes. Angled evaporation of chromium–gold (chromium work function 4.5 V) and platinum contacts (work function 5.6 V) was exploited to produce asymmetric contacts to the CNTs (work function 4.8 eV [28], [29]), as in our previous study [21]. Due to oxygen and moisture [30], the CNTs are doped p-type in ambient conditions, making holes the majority carrier type and creating a p-type Schottky barrier at the chromium contact. The resulting Schottky diodes (CNT-SDs) are similar to those of Manohara *et al.* [20]. A second photolithography step, followed by oxygen plasma etching, removed all the CNTs outside of the target device area. One of the devices is shown in Fig. 1. The close-up shows several nanotubes that extended beyond the device area and were cut by plasma etching. Contrast differences between nanotubes are due to a voltage-contrast mechanism [31] such that only nanotubes connected to the metal leads appear bright.

III. DC MEASUREMENTS

DC characterization of the 100-device array showed a diode yield under 5%, with other devices exhibiting either: 1) constant bias-independent background conductivity; 2) very high impedance; or 3) open-circuit impedance. These conditions are consistent with: 1) a metallic nanotube in the channel; 2) very high contact resistance; and 3) the absence of a contacted CNT in the device area, respectively.

Fig. 2 shows the conventional circuit model for a Schottky diode [2], in parallel with a purely reactive parasitic capacitance C_P . Here, R_S represents the series resistance of the diode circuit, in this case, the combined resistance of the CNT channel and contacts under forward bias $R_J(V)$ is the bias-dependent resistance of the Schottky junction and C_J is the capacitance across the Schottky barrier. We expect that $R_J(V)$ is determined by the Shockley diode equation

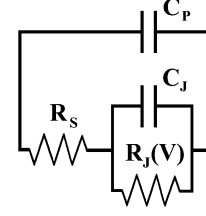


Fig. 2. Conventional circuit model for a Schottky diode shown in parallel with a parasitic capacitance C_P .

$$I(V_J) = I_0 e^{\frac{eV_J}{nkT}} - I_0$$

$$R_J(V_J) = V_J / \left(I_0 e^{\frac{eV_J}{nkT}} - I_0 \right) \quad (2)$$

where V_J is the junction voltage. It is clear that the voltage seen by the diode is equal to that applied to the parasitic capacitance. Further, rectification occurs only due to the variable junction resistance $R_J(V)$, which is expected to have an exponential dependence on applied bias. Measurements at dc exhibit this exponential dependence at low bias, followed by a linear $I - V$ characteristic at high bias, consistent with $R_J(V)$ having fallen to a negligible value, compared to a linear R_S . We can extract both resistances from the dc $I - V$ measurements.

Using the R_S and $R_J(V)$ values extracted from the $I - V$ characteristic, we calculate the fraction of applied voltage that is present as a potential drop across the Schottky junction V_J . In Fig. 3, we plot the current flowing across the junction as a function of V_J and fit the resulting data to the Shockley diode (1) for two of our CNT-SDs. The ideality factors calculated from the fits vary widely, between 2–20, indicating that although the current follows the expected exponential dependence on V_J , the mechanisms of current transport may not be the traditional thermionic emission and diffusion that limit the ideality factor to 2. Tunneling may play a significant role in these 1-D systems [32]. The value of the junction capacitance C_J ought to depend on the depletion region width. The problem of charge carrier density in a 1-D pn-junction was explored by Leonard and Tersoff [33] and Krowné [34]. Findings indicate that lack of shielding in a 1-D semiconductor leads to significantly extended charge carrier density profile. This density also depends on doping fraction, with the dominant doping in ambient CNT systems arising from oxygen and moisture [30], [35].

IV. HIGH FREQUENCY MEASUREMENTS

At high frequencies, the impedance of the parasitic capacitance $Z_p = (j\omega C_p)^{-1}$ and that of the measurement circuit (50 Ω) will determine the voltage at the CNT device terminals. The parasitic capacitance for these devices is the CPW open-circuit capacitance C_{OP} , estimated by [36]

$$C_{oc} = \frac{2\epsilon_{\text{eff}}\epsilon_0}{\pi} \left\{ K(S+W) - \left(S + \frac{2}{3}W \right) \right\} \quad (3)$$

$$K = \left\{ \left[\frac{\ln(n+n_0)}{n} + \ln\left(\frac{n_0+1}{n}\right) - \frac{1}{3} \left(\frac{1}{1+n_0} + \frac{1}{n+n_0} \right) \right] \right\} \quad (4)$$

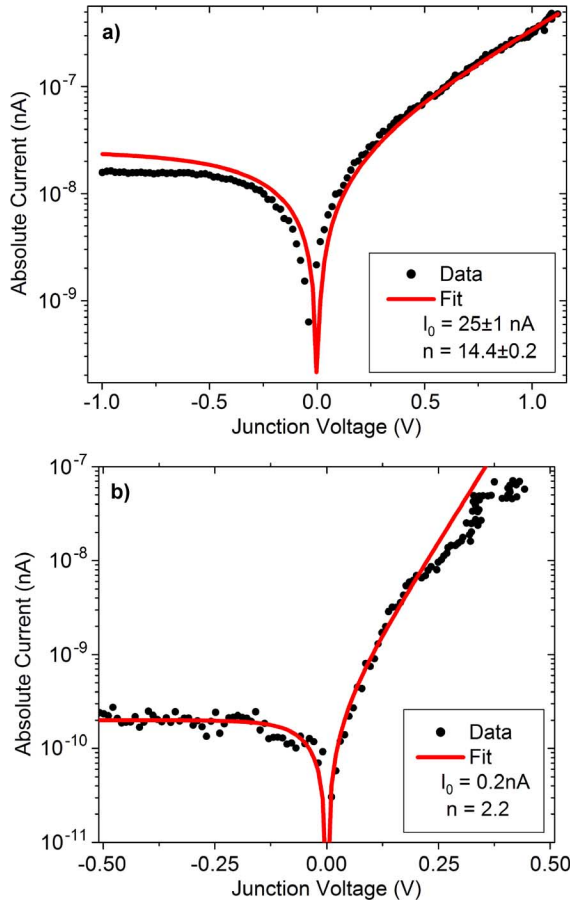


Fig. 3. Measured I - V characteristics of two CNT-SDs (black dots) with superimposed fits (red solid lines in online version) to the Shockley diode equation (1).

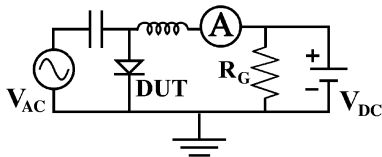


Fig. 4. Circuit diagram for the measurement setup showing the diode (DUT) connected to a bias tee (capacitor and inductor), microwave source (V_{AC}), dc source (V_{DC}), and a lock-in amplifier.

where $n_0 = \sqrt{1 + n^2}$ and $n = g/(S + W)$, ϵ_{eff} is the effective dielectric constant for the CPW, and ϵ_0 the permittivity of a vacuum. For our devices, $S = 10 \mu\text{m}$ is the inner electrode width, $W = 30 \mu\text{m}$ is the lateral separation between inner and outer CPW electrodes, and the channel length g varied between 0.5 – $25 \mu\text{m}$. The value of C_{OC} is in the range of 1 fF such that the parasitic capacitance becomes comparable to a short circuit only at frequencies above 3 THz and can thus be ignored in the frequency range studied here. This capacitance value is in agreement with the result of numerical simulations of our CPW geometry performed in Ansoft Maxwell 3D.

High-frequency measurements were performed at room temperature in a probe station using $50\text{-}\Omega$ air coplanar (ACP) microwave probes. The measurement circuit is described in Fig. 4. The CNT-SD was connected, via the microwave probe, to a broadband (50 GHz) bias tee. The ac branch was connected

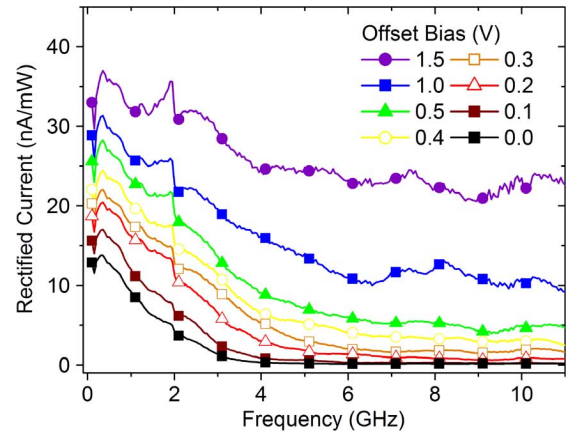


Fig. 5. Rectified current (in units of nanoamps per milliwatt) for a CNT-SD as a function of ac frequency and dc offset bias.

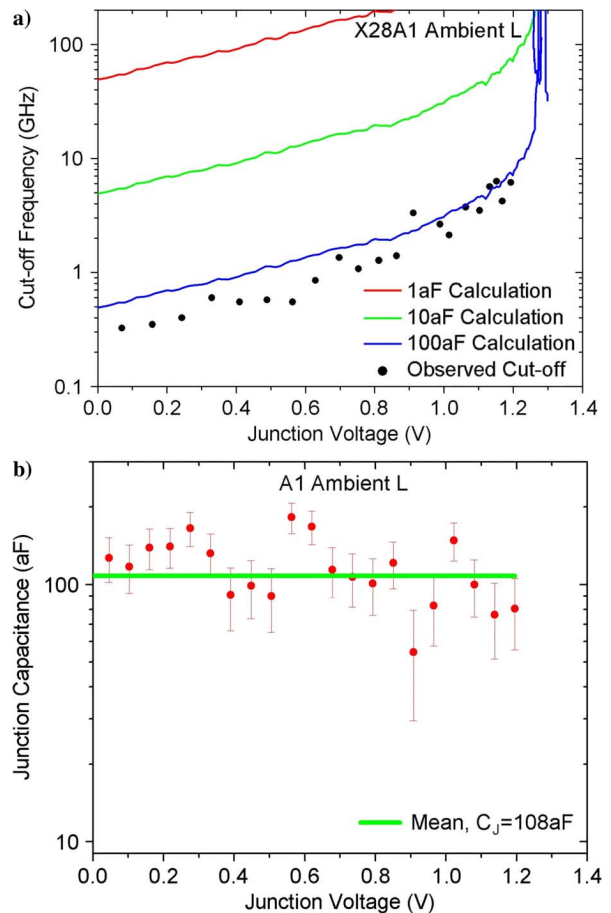


Fig. 6. (a) Calculated bias-dependent cutoff frequency $f_c(V)$ assuming various trial junction capacitance values [1 aF (in red in online version), 10 aF (in green in online version), 100 aF (in blue in online version)] and the observed cutoff frequencies (black circles) for a $20\text{-}\mu\text{m}$ -long device. (b) Experimentally determined junction capacitance as a function of frequency (red circles in online version), extracted from the observed cutoff frequency using (5). Green line (in online version) shows the mean value of the junction capacitance of 108 aF .

to a 40-GHz signal generator (V_{AC}), amplitude modulated at $f_{AM} = 200 \text{ Hz}$. The rectified current (in the dc branch) was measured with a lock-in amplifier, which had ground-isolation impedance of $10 \text{ k}\Omega$ (labeled R_G in the diagram). An offset

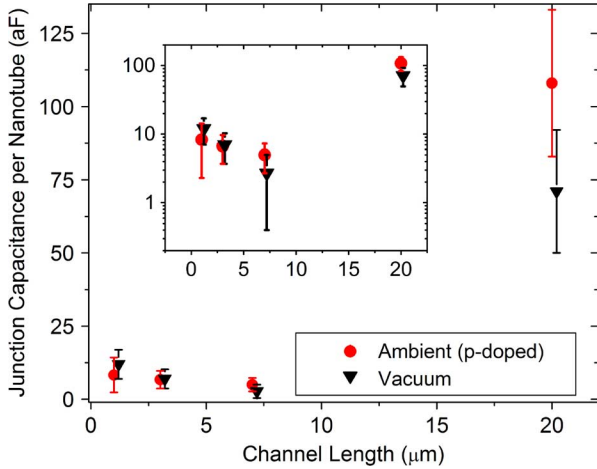


Fig. 7. Capacitance per nanotube channel as a function of device length; data are also in Table I. The vacuum values are slightly offset for clarity. Inset: Log-linear scale.

TABLE I
CHANNEL LENGTH l_{nt} , SERIES RESISTANCE R_s , DIODE IDEALITY FACTOR n , NUMBER OF NANOTUBES N , AND EXTRACTED JUNCTION CAPACITANCE C_J UNDER AMBIENT AND VACUUM CONDITIONS

Device	l_{nt} (μm)	R_s (M Ω)	n	N	Mean $C_J \pm \sigma$ (aF) (ambient)
1	20	1.38	14	1	108 ± 25
2	7	6.50	8.0	3	15 ± 7
3	1	4.30	2.2	n/a	8.3 ± 6
4	3	0.69	20	3	20 ± 9

voltage V_{DC} was applied to the CNT-SD via the low input of the amplifier.

This setup enabled control of microwave frequency and amplitude, as well as offset dc voltage. Parameter ranges studied included $100 \text{ MHz} < f < 40 \text{ GHz}$, power $-20 \text{ dBm} < P < +15 \text{ dBm}$ ($0.01\text{--}32 \text{ mW}$) and $-8 \text{ V} < V_{DC} < +8 \text{ V}$. The only calibration performed was a power-flatness calibration of the microwave source. This was done by replacing the ACP probe with a custom adapter, connected to a broadband microwave power sensor (HP 8457C). The power calibration therefore replaces the loss properties of the ACP probe with those of the simple cable adapter. The rectified current measured is therefore shown in units of amps per milliwatt of applied signal, i.e., the detectivity. Fig. 5 shows the measured detectivity of the CNT diodes as a function of frequency of the applied signal, and as a function of dc bias on the CNT. Fig. 5 shows an expected bias-dependent roll-off of detectivity in frequency. For the model circuit of Fig. 2, the bias-dependent cutoff frequency $f_c(V)$ for a Schottky diode is given by [2]

$$f_c(V) = \frac{\left(1 + \frac{R_s}{R_J(V)}\right)^{0.5}}{2\pi C_J (R_s R_J(V))^{0.5}} \quad (5)$$

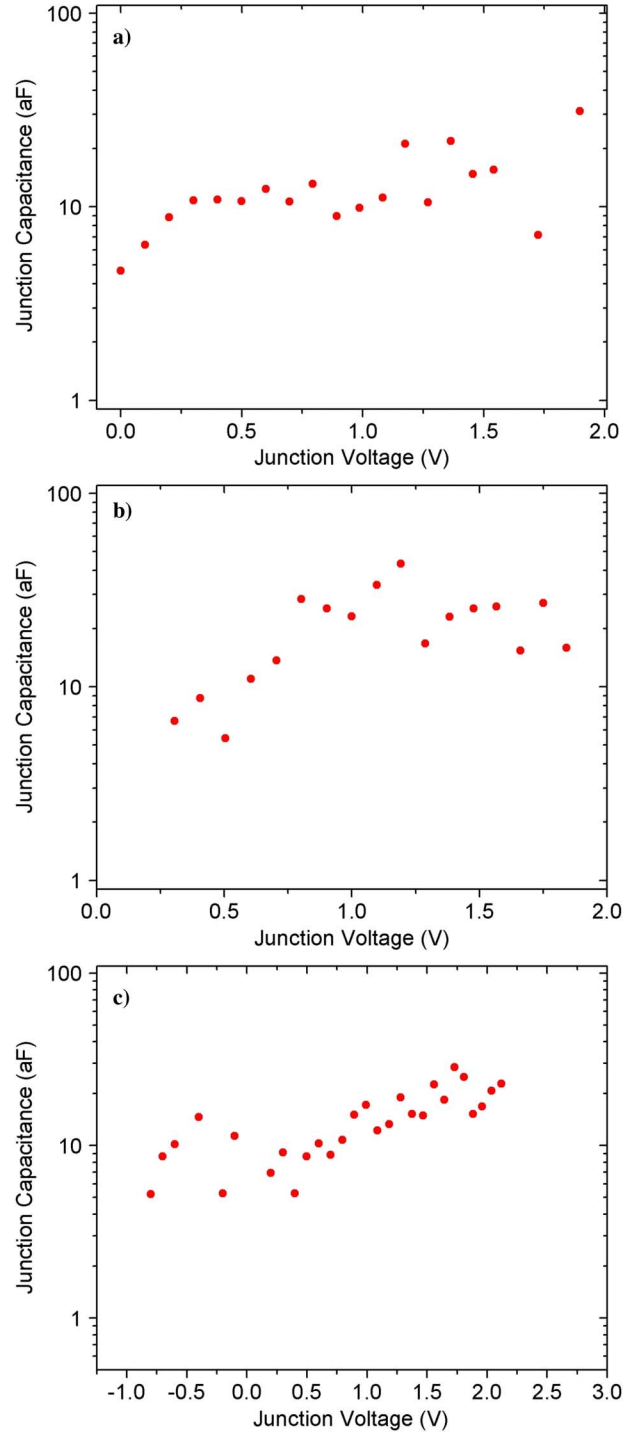


Fig. 8. Extracted junction capacitance in vacuum as a function of dc bias for CNT-SDs with channel lengths of: (a) $1 \mu\text{m}$, (b) $3 \mu\text{m}$, and (c) $7 \mu\text{m}$.

where the other terms have the same meanings as described above. The variation of the cutoff frequency with applied bias is shown in Fig. 6. As forward bias increases, the junction resistance $R_J(V)$ falls exponentially, and the combined RC time constant of the device rises to higher frequencies (in this case, from 950 MHz to 3.6 GHz for the biases shown). The measurement was repeated in ambient and vacuum (10^{-6} torr) conditions to explore the effect that oxygen and ambient moisture

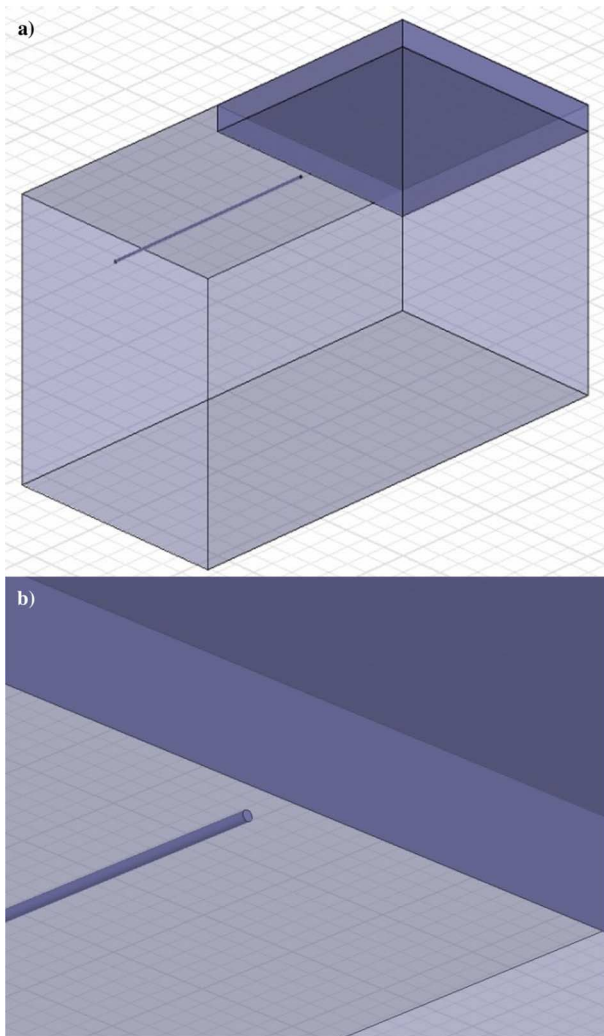


Fig. 9. 3-D model used for numerical capacitance calculations. (a) Overall view of the conducting cylinder and rectangular electrode on a quartz substrate and (b) close-up view of the gap between the channel and electrode, which represents the depletion region.

doping [30] might have on the charge carrier density and the depletion region width.

V. ANALYSIS: JUNCTION CAPACITANCE VERSUS CHANNEL LENGTH

The solid lines in Fig. 6(a) show the predictions of 5 for $f_c(V)$ for several different values of the junction capacitance C_J , superimposed on the observed cutoff frequency values (circles) for a single-CNT 20- μm -long CNT-SD. There is good agreement for bias values explored, from 0 to +1.25 V, corresponding to cutoff frequencies between 300 MHz–9 GHz, and a constant capacitance value of 108 aF. This result is shown more explicitly in Fig. 6(b), where the capacitance was extracted from the observed cutoff frequency and (4). The same measurements were performed on CNT diodes comprised of three parallel CNTs each with channel lengths of 7, 3, and 1 μm . The extracted junction capacitance values for these shorter devices were all under 20 aF despite having three parallel junctions each. As shown in Fig. 7, the capacitance per junction is found to be strongly

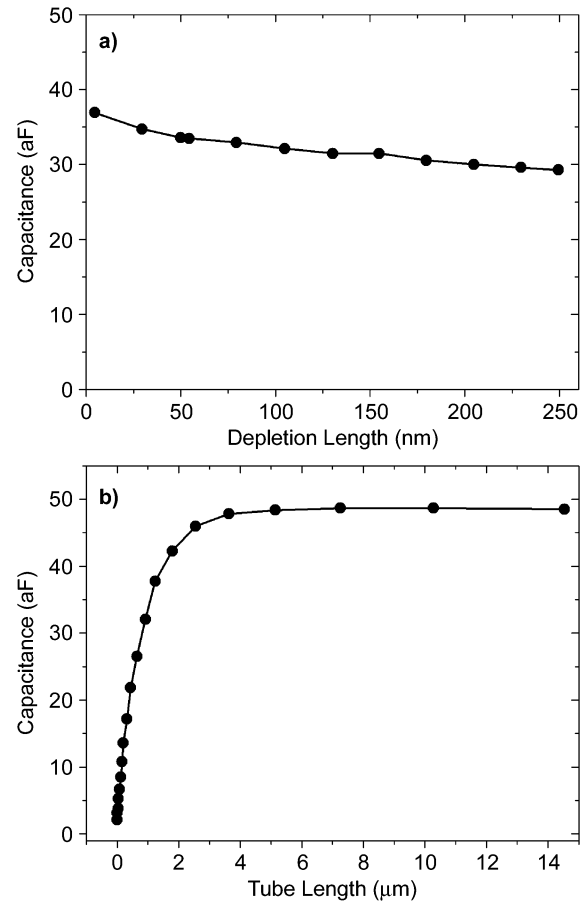


Fig. 10. Results of capacitance calculated from 3-D numerical simulations, showing a much stronger dependence on channel length than depletion length.

related to channel length, suggesting that stray capacitance between a long CNT channel and a metal electrode dominates junction capacitance in long-channel devices.

In order to explore the effect of doping, the devices were also measured under vacuum conditions (10^{-6} torr). Fig. 8 shows the junction capacitance, extracted from the observed cutoff frequencies, as a function of junction voltage [i.e., $C_J(V_J)$] for a CNT-SDs of 1-, 3-, and 7- μm channel lengths. A positive relation between capacitance and dc bias is observed.

VI. NUMERICAL SIMULATION

Numerical simulations were used to explore the relationship between channel length, depletion length, and junction capacitance. The system was modeled in Ansoft Maxwell 3-D v12 as a conducting cylinder and rectangular electrode separated by a variable gap D , representing the depletion region width, laying on top of a quartz substrate, as shown in Fig. 9. A parametric analysis was performed to vary the critical system dimensions (e.g., depletion length, tube length, etc.) and the capacitance was calculated for each solution. The calculated dependencies of junction capacitance to depletion length and nanotube channel length are shown in Fig. 10(a) and (b). Fig. 10(a) shows that capacitance is relatively insensitive to variations in depletion width, while Fig. 10(b) shows that capacitance depends strongly on the CNT length. This indicates that, for the parameters explored here, the capacitance is dominated by stray capacitance

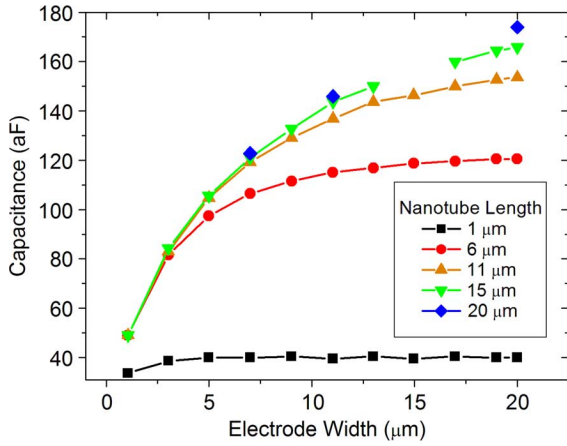


Fig. 11. Calculated capacitance values for various channel lengths as a function of electrode width.

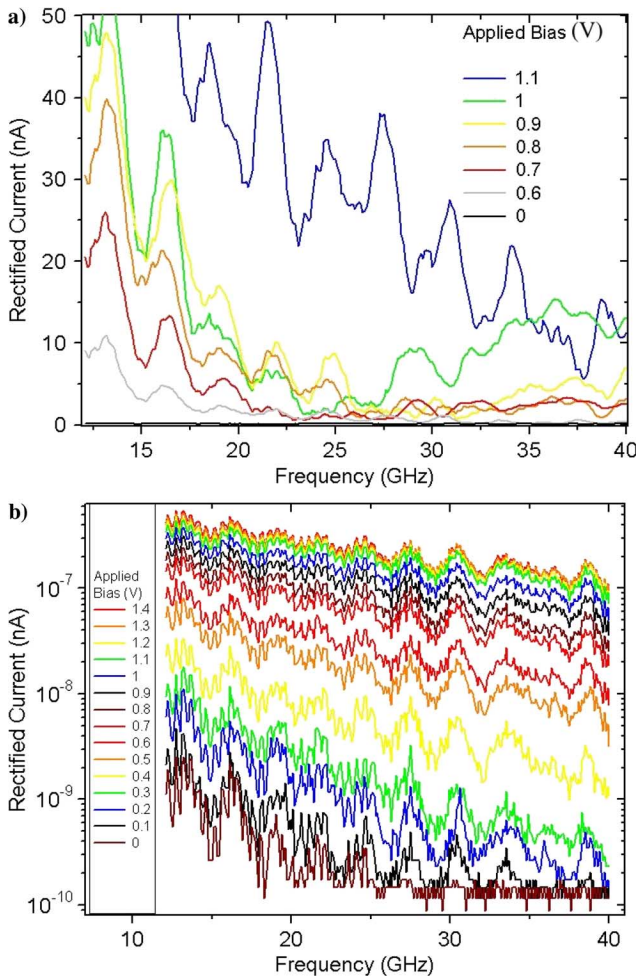


Fig. 12. Rectified current signal from a CNT-SD showing: (a) bias-dependent minima in the rectified signal at 26 GHz and (b) bias-dependent SNR of 500 at 40 GHz.

of the CNT length to the electrode. Fig. 10(b) also shows that the capacitance saturates for long CNT lengths. This is further explored in Fig. 11, where calculations were performed with different electrode widths. The CNT length at which saturation

occurs is seen to scale with electrode width. These results support our hypothesis that stray capacitance dominates junction capacitance in long-channel devices.

The junction voltage-dependent capacitances in vacuum (Fig. 8) do show a slight increasing dependence of capacitance on junction voltage, as expected for narrowing of the depletion width with voltage. The observation of this effect in devices in vacuum likely indicates that doping by ambient species reduces the depletion width to small values in ambient [35], and removal of doping in vacuum allows the depletion width to be modulated more significantly by bias voltage.

VII. HIGH-FREQUENCY TRANSPORT

Finally, the rectified signal was used to probe transport up the equipment limit of 40 GHz. Fig. 12 shows two examples of very high-frequency rectification. The large peaks in the rectified signal with periodicity of ~ 3 GHz correspond to resonances in the microwave probe assembly that were not calibrated out by the power flatness calibration. Nevertheless, two important facts can be gleaned from the data. Fig. 12(a) shows a minimum in the rectified signal at -1.0 - and -1.1 -V dc bias and 25 GHz, followed by a recovery of rectification at higher frequencies. This phenomenon is not understood, but serves as an example of the utility of this technique in examining unusual phenomena in RF 1-D transport. Fig. 12(b) shows data from a CNT-SD at frequencies up to 40 GHz. The bias dependence reveals a noise floor of 0.2 nA and a maximum signal of 100 nA at 40 GHz, yielding an SNR of 500:1.

VIII. CONCLUSION

We have demonstrated the use of Schottky rectification as a probe of high-frequency electrical transport in high-impedance semiconducting nanosystems. We expect this technique will be particularly useful for 1-D systems (semiconducting CNTs and small semiconducting nanowires) because these systems exhibit quantized conductance and cannot be impedance matched to macroscopic RF equipment. We have used this technique to examine the capacitance of CNT Schottky barriers as a function of bias and ambient pressure and doping. We find that the capacitance of long-channel CNT-SDs is dominated by stray capacitance between the metal electrode and the bulk of the nanotube channel and exhibits no dependence on dc bias, in agreement with numerical simulations. For short-nanotube diodes with doping reduced in vacuum, we find junction capacitance values under 10 aF, which exhibit a positive relation with forward bias, consistent with the hypothesis of increasing Schottky barrier capacitance as the length of the depletion region decreases.

We expect that these measurements could be significantly improved by calibrating the power reaching the device. By using a $50\text{-}\Omega$ load fabricated in a CPW geometry on a quartz substrate, it would be possible to calibrate out the microwave probe assembly’s transmission resonances and get a clearer picture of the frequency response of the CNT-SD devices out to 40 GHz or beyond. Furthermore, improvement of the series resistance should be possible by doping, cleaner fabrication methods, and by annealing the contact. Such improvements, combined with the Schottky barrier capacitances of 10 aF, point

to the possibility of single-tube CNT-SDs with bandwidths exceeding 100 GHz. Low-temperature measurements would also clarify the transport mechanism at the barrier while simultaneously providing a longer mean-free path to enable detection of Fermi or Luttinger liquid plasmon velocity resonances.

With stray capacitances of order 10 aF or greater and junction resistance necessarily larger than 6 k Ω , it is unlikely that the cutoff frequency of a single-nanotube device will exceed 1 THz. However, the stray capacitance will scale sub-linearly with the number of tubes, while the junction resistance and series resistance should scale inversely with tube number. Thus, bundles or parallel arrays of CNTs [18], [19] could show an even higher cutoff frequency.

REFERENCES

- [1] H. Ajiki and T. Ando, "Electronic states of carbon nanotubes," *J. Phys. Soc. Jpn.*, vol. 62, no. 4, pp. 1255–1266, Apr. 1993.
- [2] A. M. Cowley and H. O. Sorensen, "Quantitative comparison of solid-state microwave detectors," *IEEE Trans. Microw. Theory Tech.*, vol. MTT-14, no. 12, pp. 588–602, Dec. 1966.
- [3] P. McEuen, M. Fuhrer, and H. Park, "Single-walled carbon nanotube electronics," *IEEE Trans. Nanotechnol.*, vol. 1, no. 1, pp. 78–85, Mar. 2002.
- [4] T. Durkop *et al.*, "Extraordinary mobility in semiconducting carbon nanotubes," *Nano Lett.*, vol. 4, no. 1, pp. 35–39, Jan. 2004.
- [5] M. S. Purewal *et al.*, "Scaling of resistance and electron mean free path of single-walled carbon nanotubes," *Phys. Rev. Lett.*, vol. 98, no. 18, May 2007, Art. ID 186808.
- [6] T. Ghanem, "Electronic transport in low dimensions: Carbon nanotubes and mesoscopic silver wires," Ph.D. dissertation, Phys. Dept., Univ. Maryland at College Park, College Park, MD, 2008.
- [7] C. Rutherglen and P. Burke, "Nanoelectromagnetics: Circuit and electromagnetic properties of carbon nanotubes," *Small*, pp. 884–906, Apr. 20, 2009.
- [8] S. Tomonaga, "Remarks on Bloch's method of sound waves applied to many-fermion systems," *Progr. Theoret. Phys.*, vol. 5, no. 4, pp. 544–569, 1950.
- [9] J. M. Luttinger, "An exactly soluble model of a many-fermion system," *J. Math. Phys.*, vol. 4, no. 9, pp. 1154–1162, 1963.
- [10] R. Tarkiainen *et al.*, "Multiwalled carbon nanotube: Luttinger versus Fermi liquid," *Phys. Rev. B, Condens. Matter*, vol. 64, no. 19, Nov. 2001, Art. ID 195415.
- [11] M. Bockrath *et al.*, "Luttinger-liquid behaviour in carbon nanotubes," *Nature*, vol. 397, no. 6720, pp. 598–601, Feb. 1999.
- [12] P. J. Burke, "Luttinger liquid theory as a model of the gigahertz electrical properties of carbon nanotubes," *IEEE Trans. Nanotechnol.*, vol. 1, no. 3, pp. 129–144, Sep. 2002.
- [13] D. Dragoman and M. Dragoman, "Terahertz continuous wave amplification in semiconductor carbon nanotubes," *Phys. E, Low-Dimensional Syst. Nanostruct.*, vol. 25, no. 4, pp. 492–496, Jan. 2005.
- [14] D. Dragoman and M. Dragoman, "Terahertz oscillations in semiconducting carbon nanotube resonant-tunneling diodes," *Phys. E, Low-Dimensional Syst. Nanostruct.*, vol. 24, no. 3–4, pp. 282–289, Sep. 2004.
- [15] A. Akturk *et al.*, "Terahertz current oscillations in single-walled zigzag carbon nanotubes," *Phys. Rev. Lett.*, vol. 98, no. 16, Apr. 2007, Art. ID 166803.
- [16] P. J. Burke, "AC performance of nanoelectronics: Towards a ballistic THz nanotube transistor," *Solid State Electron.*, vol. 48, no. 10–11, pp. 1981–1986, Oct.–Nov. 2004.
- [17] C. Rutherglen, D. Jain, and P. Burke, "Nanotube electronics for radiofrequency applications," *Nature Nanotechnol.*, vol. 4, no. 12, pp. 811–819, Dec. 2009.
- [18] A. A. Pesetski *et al.*, "Carbon nanotube field-effect transistor operation at microwave frequencies," *Appl. Phys. Lett.*, vol. 88, no. 11, Mar. 2006, Art. ID 113103.
- [19] L. Nougaret *et al.*, "80 GHz field-effect transistors produced using high purity semiconducting single-walled carbon nanotubes," *Appl. Phys. Lett.*, vol. 94, no. 24, Jun. 2009, Art. ID 243505.
- [20] H. M. Manohara *et al.*, "Carbon nanotube Schottky diodes using Ti-Schottky and Pt-ohmic contacts for high frequency applications," *Nano Lett.*, vol. 5, no. 7, pp. 1469–1474, Jul. 2005.
- [21] E. Cobas and M. S. Fuhrer, "Microwave rectification by a carbon nanotube Schottky diode," *Appl. Phys. Lett.*, vol. 93, no. 4, Jul. 2008, Art. ID 043120.
- [22] H. W. C. Postma *et al.*, "Carbon nanotube single-electron transistors at room temperature," *Science*, vol. 293, no. 5527, pp. 76–79, Jul. 2001.
- [23] P. Jarillo-Herrero *et al.*, "Electron-hole symmetry in a semiconducting carbon nanotube quantum dot," *Nature*, vol. 429, no. 6990, pp. 389–392, May 2004.
- [24] N. Yoneya *et al.*, "Coulomb blockade in multiwalled carbon nanotube island with nanotube leads," *Appl. Phys. Lett.*, vol. 79, no. 10, pp. 1465–1467, Sep. 2001.
- [25] Y. C. Tseng and J. Bokor, "Characterization of the junction capacitance of metal-semiconductor carbon nanotube Schottky contacts," *Appl. Phys. Lett.*, vol. 96, no. 1, Jan. 2010, Art. ID 013103.
- [26] C. Kocabas *et al.*, "High-frequency performance of submicrometer transistors that use aligned arrays of single-walled carbon nanotubes," *Nano Lett.*, pp. 1937–1943, May 2009.
- [27] A. Rutkowska *et al.*, "Horizontal alignment of chemical vapor-deposited SWNTs on single-crystal quartz surfaces: Further evidence for epitaxial alignment," *J. Phys. Chem. C*, vol. 113, no. 39, pp. 17087–17096, Oct. 2009.
- [28] S. Suzuki *et al.*, "Work functions and valence band states of pristine and Cs-intercalated single-walled carbon nanotube bundles," *Appl. Phys. Lett.*, vol. 76, no. 26, pp. 4007–4009, Jun. 2000.
- [29] S. Suzuki *et al.*, "Work functions of individual single-walled carbon nanotubes," *Appl. Phys. Lett.*, vol. 85, no. 1, pp. 127–129, Jul. 2004.
- [30] C. M. Aguirre *et al.*, "The role of the oxygen/water redox couple in suppressing electron conduction in field-effect transistors," *Adv. Mater.*, vol. 21, no. 30, pp. 3087–3091, Aug. 2009.
- [31] T. Brintlinger *et al.*, "Rapid imaging of nanotubes on insulating substrates," *Appl. Phys. Lett.*, vol. 81, no. 13, pp. 2454–2456, Sep. 2002.
- [32] S. N. Mohammad, "Contact mechanisms and design principles for (Schottky and ohmic) metal contacts to semiconductor nanowires," *J. Appl. Phys.*, vol. 108, no. 3, Aug. 2010, Art. ID 034311.
- [33] F. Leonard and J. Tersoff, "Novel length scales in nanotube devices," *Phys. Rev. Lett.*, vol. 83, no. 24, pp. 5174–5177, Dec. 1999.
- [34] C. M. Krowne, "Nanowire and nanocable junction capacitances: Results for metal and semiconducting oxides," *Phys. Lett. A*, vol. 374, no. 9, pp. 1172–1179, Feb. 2010.
- [35] Y. F. Chen and M. S. Fuhrer, "Tuning from thermionic emission to ohmic tunnel contacts via doping in Schottky-barrier nanotube transistors," *Nano Lett.*, vol. 6, no. 9, pp. 2158–2162, Sep. 2006.
- [36] R. M. Simons, *Coplanar Waveguide Circuits, Components and Systems*. New York: Wiley, 2001.

Enrique D. Cobas, photograph and biography not available at time of publication.

Steven M. Anlage (A'95–M'08), photograph and biography not available at time of publication.

Michael S. Fuhrer, photograph and biography not available at time of publication.